LOADING AND ASYMMETRY MEASUREMENTS AND MODELING FOR THE NSTX ICRF SYSTEM

D. W. Swain[1], M. D. Carter[1], J. R. Wilson[2], P. M. Ryan[1],
J. B. Wilgen[1], J. Hosea[2], A. Rosenberg[2]

[1] *Oak Ridge National Laboratory, Oak Ridge, TN*

[2] *Princeton Plasma Physics Laboratory, Princeton, NJ*

Abstract

The ion cyclotron heating and current drive system on NSTX has operated with the full 12-antenna, 6-transmitter configuration, delivering over 3 MW reliably for pulse lengths over 100 ms with various phasings of the antenna system. A circuit model of the full 12-antenna coupled system has been developed that gives good agreement with vacuum measurements. When it is used to extract the effects of the plasma on the rf circuit, pronounced asymmetries in antenna loading are observed, even when antenna phasing is symmetrical (e.g., 0π0π0π…..). The loading of the plasma on the antenna has been calculated with the RANT3D code using measured edge density profiles in front of the antenna; these agree with measured loading values. The asymmetry is caused primarily by the large pitch angle of the magnetic field in front of the antenna, coupled with the gradients in the plasma edge.

1. Introduction

The National Spherical Torus Experiment (NSTX)[1] is a small-aspect-ratio machine (R_0 = 0.85 m, a = 0.65 m) in operation at PPPL. It has a 6-MW, 30-MHz ion cyclotron system[23] to heat the plasma and to drive current. Twelve antenna current straps are mounted vertically on the outer wall at the machine midplane (see **Fig. 1**). The antenna array subtends almost 90° toroidally.

While the NSTX plasma is similar to a standard tokamak plasma in many respects, the operation of the rf system is different in some key aspects:

- The magnetic field is relatively low (0.3 – 0.6 T at the center, 0.1 – 0.3 T at the outside edge), so the system operates at a high harmonic of the ion cyclotron frequency ($\omega/\omega_{ci} \geq 10$).
- Because of the relatively high values of $B_{poloidal}/B_{toroidal}$ in typical spherical torus operation, the pitch angle of the magnetic field in front of the antennas is usually at a large angle (from 20° to over 45°) relative to the horizontal.
- NSTX operates at densities of 1 – 5 x 10^{19} m^{-3}; coupled with the low field values, this results in the perpendicular components of the plasma dielectric tensor being very large, of order 10^4 (i.e., $\omega_p^2/\omega_c^2 >> 1$).

These differences, in particular the large pitch angle, cause a significant increase in the influence of the plasma on the antenna system, introducing a large measured toroidal asymmetry into the rf system characteristics. Earlier work[4] has indicated the presence of this asymmetry; this paper studies the effects as plasma parameters are varied and does a detailed comparison with theoretical modeling for a number of different plasma conditions. The changes can be explained by a 3D modeling of the antenna and plasma. We obtain good agreement between theory and experiment, with no adjustable parameters, when the measured density profiles and magnetic field geometry are used in the calculations.

While this asymmetry will exist to some extent in all tokamaks, the large pitch angle makes it very significant in NSTX, and it should be equally so in other spherical torii. In practice, this effect can cause a factor of two difference in plasma loading of the antenna as the antenna phasing is changed.

This paper is divided into the following sections: Sec. 2 describes the rf system in more detail and Sec. 3 describes a new technique for measuring the S-matrix of the system in the presence of plasma. Sec. 4 describes the calculation of the S-matrix using results from the RANT3D[5] and GLOSI[6] codes, and Sec. 5 shows a comparison of the measurements with the theory and the variation of the S-matrix elements with different plasma conditions. Section 6 discusses the physics origin of the asymmetry, and Sec. 7 presents a practical application of the results to compute the effective loading for a current-drive experiment that has been performed.

2. Description of the rf system

A schematic diagram of the NSTX rf system is shown in **Fig. 2**. The 12 antennas are connected in six resonant loops, with antennas 1 and 7 being in one loop, 2 and 8 in another, etc. Each loop consists of two antenna current straps, each connected to a vacuum feedline and feedthrough, followed by a length of pressurized 6-in-diameter, 50-Ω characteristic impedance coaxial transmission line. The junction of the two lines from the current straps is the drive point of the resonant loop. The *electrical length* of the drive point is 3λ/4 from the ground of one strap and 5λ/4 from the ground of the other strap, resulting in the drive point being located at a high-voltage point in the resonant loop. The loops were adjusted with no plasma present to be exactly 2 wavelengths long electrically, so that the impedance looking into each drive point was real; this was done while all the other loops were shorted to ground at their drive points, thereby destroying their resonant nature and minimizing their effect on the resonance of the loop being adjusted. The straps are oriented so that the currents in the straps at opposite ends of a single loop are out of phase (i. e., the current in strap 7 has a phase of π radians relative to strap 1).

Throughout the rest of the paper, we will be discussing the radio-frequency scattering matrix **S**. The S-matrix elements are defined as $S_{kj} = b_j/a_k$, where a_k is the amplitude of a forward wave on port k of an n-port system, and b_j is the wave traveling out of port j as a result of the forward wave into port k.[7] In vector notation, $\boldsymbol{b} = \mathbf{S} \bullet \boldsymbol{a}$, where $\boldsymbol{a}$ and $\boldsymbol{b}$ are n-element vectors of forward and reflected voltage, respectively, and **S** is an n x n (complex) matrix. We calculate two S-matrices in the paper: the twelve antennas have a 12 x 12 S-matrix, while the six inputs to the resonant loops are characterized by a 6 x 6 S-matrix. If the antenna S-matrix is known, then the loop S-matrix can be calculated using standard transmission line equations, as described later.

Since the straps are closely adjacent to each other they have significant mutual inductive coupling, with the mutual inductance being about 10% of the self-inductance of the straps. Decouplers are installed between the six drive points as shown in **Fig. 2** to decouple the loops from each other electrically. The decouplers are lengths of 91 Ω coax with a reactive element at the midpoint. By adjusting the lengths of the coax and the value of the reactive elements, the 6 x 6 S-matrix seen looking into the six drive points was made to have diagonal components that had zero imaginary parts, and the first off-diagonal components were set to zero. The further off-diagonal components (e.g., S_{31}) are non-zero, but relatively small (measured inter-strap coupling for non-adjacent straps is ≤ 1%). The decoupler adjustments were made with no plasma present; as we shall see, the presence of the plasma significantly changes the inter-loop coupling.

A piece of 74.5-Ω coaxial line 2.5 m long (= λ/4 at 30 MHz) is connected to the drive point of each decoupler. These act as quarter-wave transformers to partially pre-match the impedances at the loop/decoupler junctions to the 50-Ω main transmission line. On each line there is a long length of pressurized 9" coax, connected to a conventional line-stretcher and stub matching system.

Forward and reflected power and their relative phase in each main transmission line are measured on the matched side of the stub as shown in **Fig. 2**. Using the known stub and line lengths, these measurements are translated along each line, through the quarter-wave-transformer, to the junction of the line with the decouplers and resonant loop. In addition, there is a direct measurement of the rf voltage amplitude and phase at this junction.

3. Experimental determination of the S-matrix

We want to determine the values of the elements in the 6 x 6 S-matrix at the connection between the resonant loops and the decouplers for different sets of plasma conditions, to compare the measured values with calculations. From the formula $\boldsymbol{b} = \mathbf{S} \bullet \boldsymbol{a}$, one measurement of $\boldsymbol{a}$ and $\boldsymbol{b}$ does not give enough information to determine **S.** However, six measurements in which the six $\boldsymbol{a}$-vectors are linearly independent will give enough information. We can write $\mathbf{B} = \mathbf{S} \bullet \mathbf{A}$ and then $\mathbf{S} = \mathbf{B} \bullet \mathbf{A}^{-1}$, where **B** and **A** are 6 x 6 matrices made up of the six $\boldsymbol{b}$ and $\boldsymbol{a}$ vectors, respectively.

We obtained the six linearly independent measurements by firing each of the six transmitters sequentially for a short (≈ 5 ms) rf pulse. The top plot of **Fig. 3** shows the forward power signals from all six transmitters vs. time, in which the six transmitters are fired sequentially. The lower plot shows the reflected power vs. time. Note that the measured forward power signals on the unpowered lines, although small, are not zero. This is because the reflected power on an unpowered line travels to the unpowered transmitter, where it is then reflected back toward the antenna array and appears as a forward power (i.e., $P_{refl} \approx P_{fwd}$ on the undriven lines). The six $\boldsymbol{b}$ and $\boldsymbol{a}$ vectors at the resonant loop junctions can be computed and the matrix inversion performed to obtain **S**.

A necessary condition for this technique to work is that *the plasma must remain unchanged* during the approximately 36 ms that the pulsed measurements are made. We monitor several plasma parameters (e.g., plasma position and current, line-averaged density, stored energy) to assure that this is a good assumption. Nevertheless, there is some noise on the reflected power traces (as seen in **Fig. 3**) caused by turbulence in the plasma edge[8] that limits the accuracy of the measurements. Because of the noise, only the elements of the S-matrix on or adjacent to the diagonal can be calculated with any accuracy; the further off-diagonal elements (whose values are normally only a few percent) are swamped by the measurement inaccuracies from plasma fluctuations.

Results from this technique are shown in **Figs. 4 and 5** for a typical shots with and without plasma. **Figure 4** shows the magnitude of the six diagonal components of **S**, $S_{diag} = |S_{i,i}|$ just on the transmitter side of the decouplers vs. line number for the two cases. For the vacuum case, the losses in the system are low, corresponding to the losses in the resonant circuit with no plasma loading, so the values of S_{diag} are near unity as expected. For the plasma case, the values of S_{diag} are lower because of the loading of the antennas by the plasma. As can be seen, the values of S_{diag} vary only slightly from line to line, both for the plasma and vacuum cases. From the value of S_{diag}, the plasma loading on each current strap R' (the resistive loss/unit length on the strap) can

be computed using a coupled circuit model of the antenna/resonant loop structure. Results are given in **Sec. 5**.

Figure 5 shows the magnitudes of the elements of **S** just above and below the diagonal of the matrix, S_{pos} and S_{neg}, defined as $|S_{i+1,i}|$ and $|S_{i,i+1}|$ respectively, for the same vacuum and plasma cases. Since the decouplers were adjusted to counterbalance the inter-loop coupling between nearest neighbors, the values for the vacuum case (dashed curves) should be very near to zero. We see that this is the case; for $i = 1 - 3$ the values are typically ≤ 0.01. For $i = 4$ and 5 the values go up to about 0.03, indicating the approximate limits of resolution of this technique.

The values of S_{pos} and S_{neg} when plasma is present are non-zero and quite different, with S_{pos} being about twice S_{neg}. This indicates both the change in inter-loop coupling introduced by the plasma *and* the asymmetry in the S-matrix. The reason for this change is explained in the next section.

4. Calculation of the S-matrix using GLOSI and RANT3D

The RANT3D code is used to calculate the coupling of realistic-geometry antennas to the plasma. It computes the fields in the vacuum cavity and out to the plasma, and also calculates the effects of the plasma on the antenna electrical characteristics (e.g., loading, mutual inductance, etc.). The code makes the following approximations:

- It assumes planar geometry for the antenna straps and cavity, and a slab model for the plasma that is inhomogeneous in the x (radial) direction but is uniform in y (poloidal) and z (toroidal) directions.
- It models all 12 straps of the antenna, with values of strap and antenna cavity dimensions close to those of the actual experiment (see **Fig. 6**).
- It uses the measured plasma density profile for the density n(x) that goes into the plasma dispersion function. The edge profile near the antenna is measured using a microwave reflectometer positioned between two of the antennas in the array.[9]
- Poloidal and toroidal magnetic fields $B_y(x)$ and $B_z(x)$ are obtained from EFIT reconstructions of the plasma equilibrium.[10]

The GLOSI code is used to compute the impedance in Fourier space at the plasma "edge", where the vacuum fields calculated in RANT3D are matched to the fields in the plasma.

RANT3D/GLOSI is used to calculate a 12 x 12 impedance matrix (Z-matrix) that gives the electrical properties of the 12 current straps in the presence of plasma. The method used is:

1. Set up coupled antenna structure in RANT3D, with multiple current straps.
2. Run GLOSI to compute the plasma input impedance in Fourier space at the plasma "boundary", given density profiles and magnetic field profiles and angles.
3. Specify the currents on each strap, and assume that they are UNIFORM poloidally, (v_{phase} infinite).
4. Run RANT3D to calculate the electric fields E everywhere, in particular at the strap locations.
5. Define the power from each strap to be $P_k = 0.5 \int (E \quad J_k)$, where the integral is taken over the strap height. Because of the assumption that J is uniform poloidally, this can be written
$$P_k = 0.5 J_k \int \sum_j E_{kj} = 0.5 J_k (\sum_j Z_{kj} J_j)$$
6. By carrying out the calculation of P_k for special cases, the Z-matrix elements can be evaluated:

- Set only one current non-zero, so $P_k = 0.5\, Z_{kk}\, J_k^2$ gives the diagonal terms of Z.
- Set only two currents non-zero, so $P_k = 0.5\, (Z_{kk}\, J_k^2 + Z_{kj}\, J_k\, J_j)$, use Z_{kk} from above to subtract and obtain Z_{kj} for k ≠ j.
- Repeat above for all pairs of currents.

The Z-matrix gives the relationship between the current and voltage at the inputs to an *n*-port system: $\boldsymbol{V} = \mathbf{Z} \bullet \boldsymbol{I}$, where $\boldsymbol{I}$ is the vector of currents going into the ports, and $\boldsymbol{V}$ is the corresponding vector of voltages. The relationship between the Z-matrix and the S-matrix is given by

$$\mathbf{S} = (\mathbf{Z}/Z_0 - \mathbf{U})^{-1} \bullet (\mathbf{Z}/Z_0 + \mathbf{U})$$

where $\mathbf{U}$ is an n x n identity matrix and Z_0 is the characteristic impedance of the transmission lines (50 Ω in our case).

The magnitude of a 12 x 12 antenna S-matrix for a typical plasma case and for a vacuum case are shown in **Fig. 7**. Note the significant asymmetry in the matrix with plasma. In the absence of plasma, the S-matrix is symmetric, both from measurements and also as calculated by RANT3D.

Once the 12 x 12 Z-matrix of the antennas has been computed, the 6 x 6 S-matrix of the loops can be calculated using a coupled transmission line model. Dividing the elements of $\mathbf{Z}$ by the length of the current straps gives the impedance matrix per unit length, $\mathbf{Z'}$ for the straps. This matrix is then used in the coupled-circuit transmission line equations:

$$d\boldsymbol{V}/dx = \mathbf{Z'} \bullet d\boldsymbol{I}/dt = j\omega\, \mathbf{Z'} \bullet \boldsymbol{I}$$

$$d\boldsymbol{I}/dx = j\omega \mathbf{C'} \bullet \boldsymbol{V} = j\omega C'\, \boldsymbol{V}$$

where $\boldsymbol{V}(x)$ and $\boldsymbol{I}(x)$ are the 12-vectors of current and voltage along the 12 antenna straps, $\mathbf{Z'}$ is from RANT3D, and $\mathbf{C'}$ is a diagonal capacitance matrix (inter-strap capacitive coupling is very small because of the Faraday shields on the antennas, so the matrix is represented by a diagonal matrix with constant values of C' for all straps, determined primarily by the capacitance per unit length between the antenna strap and the Faraday shield). Using the above equations for the currents and voltages on the antenna straps, a circuit model of the resonant loops can be made that includes the lengths of 50-Ω transmission lines running from the current straps to the junction with the drive lines. This model yields the 6 x 6 S-matrix seen at the input to the resonant loops and decoupler junction. The components of this calculated S-matrix will be compared in **Sec. 5** with the values determined from the experimental data using the technique described in **Sec. 3**.

5. Comparison of measurements and calculations of the S-matrix with plasma

The experiments were carried out with plasma currents of 300 kA and 800 kA (giving magnetic field pitch angles at the antenna of about 18° and 35°, respectively), with a vacuum magnetic field on axis of B_0 = 0.45 T. Central density scans were done with n_0 = 1.5 – 4.5 x 10^{19} m^{-3} for I_p = 300 kA, and n_0 = 4.0 – 6.0 x 10^{19} m^{-3} for I_p = 800 kA. The "outer gap" (distance from the Faraday shield to the outermost closed flux surface, from the EFIT magnetics equilibrium code) was varied to obtain data for different plasma profiles near the antenna.

In NSTX, the 30-MHz wave that is launched begins to propagate in the plasma for relatively low values of density (few 10^{18} m^{-3}, exact value depending on the k_z value of the launched wave). In addition, the density profile shapes for the 300 and 800 kA currents were quite different, with the 300 kA profiles being more peaked. For these reasons we re-defined the "gap" to be the distance

from the Faraday shield to where the density is 4 x 10^{18} m^{-3}. This gave much more consistent results in both the experimental and theoretical plots.

Plasma loading (diagonal terms of S)

The response of the diagonal term of **S** is as expected, decreasing S_{diag} from around unity in vacuum to between 0.5 and 0.8 with plasma (see **Fig. 4),** and yields the plasma load resistance through circuit analysis. In addition to decreasing the magnitude of S_{diag}, the presence of plasma decreases the effective strap inductance; this increases the resonant frequency of the loop and S_{diag}, at the junction is no longer purely real but has an imaginary component. **Figure 8** shows the behavior of the magnitude and phase angle of S_{diag}, vs. the outer gap distance. The points with error bars are from the analysis of the rf signals, while the lines are from RANT3D runs using density profiles similar to those measured in the experimental run. As can be seen, the results are relatively independent of the plasma current, and appear to depend primarily on the density profile near the antenna.

The values of *R'* corresponding to the data plotted in **Fig. 8** are shown in **Fig. 9**. Although there is reasonable agreement given the measurement error bars, the measured values are somewhat higher than the calculations from RANT3D. **Figure 9** also shows the inductance of the strap relative to its vacuum value. The effective inductance decreases as the gap decreases, both in the analysis of the rf data and in the model, in agreement with expectations.

Inter-loop coupling (off-diagonal components of S)

Figure 10 plots the magnitude of S_{pos} and S_{neg} vs. gap, for I_p= 800 kA and 300 kA. Significant asymmetry is observed in the measurements: $S_{pos} \geq 3\ S_{neg}$ for the 800 kA case, and $S_{pos} \approx 2\ S_{neg}$ for the 300 kA case. There is good agreement between experiment and theory for small gaps. For large gaps we expect the magnitude of the components of **S** to decrease with distance, since for the vacuum case $|S_{pos}| = |S_{neg}| = 0$. The calculated curves decrease faster than the measured data. However, the calculated values depend fairly sensitively on details of the density profile, so it is difficult to get results that are in exact agreement with experiment. Nevertheless, the relative constancy of S_{pos} and S_{neg} with gap is puzzling. While it is most likely that this is caused by experimental inaccuracies, there is a possibility that it is caused by some effect that is not included in this analysis.

6. Discussion of the asymmetry

There is an up-down loading asymmetry in the plasma wave dispersion equation when gradients are taken into account. Assuming that $E_z \approx 0$ (because of the high parallel conductivity of the plasma) but including a gradient in the *x* (radial) direction, a second-order differential equation for the rf electric field $E_y(x)$ can be derived :

$$\frac{A(n_y,n_z,x)}{k_0{}^2}\frac{d^2E_y}{dx^2}+\frac{B(n_y,n_z,x)}{k_0}\frac{dE_y}{dx}+C(n_y,n_z,x)E_y=0$$

where $n_y = k_y/k_0$, $n_z = k_z/k_0$ are the indices of propagation in the y and z directions, respectively, $k_0 = \omega/c$, and the coordinates are in the local reference frame (z-direction parallel to the local magnetic field). *A*, *B*, and *C* are functions of the dielectric tensor components for the plasma; for a cold plasma the only two terms that appear are *S(x)* and *D(x)*, which are the perpendicular and off-diagonal cross-term of the dielectric tensor in the Stix notation,[11] and are functions of *x* through the varying density and magnetic field. The coefficients are:

$$A(n_y, n_z, x) = \frac{n_z^{\,2} - S(x)}{n_y^{\,2} + n_z^{\,2} - S(x)}$$

$$B(n_y, n_z, x) = -n_y^{\,2}\,\frac{dS(x)/dx}{n_y^{\,2} + n_z^{\,2} - S(x)}$$

$$C(n_y, n_z, x) = -\frac{n_y}{n_y^{\,2} + n_z^{\,2} - S(x)}\left[\frac{dD(x)}{dx} + \frac{D(x)\dfrac{dS(x)}{dx}}{n_y^{\,2} + n_z^{\,2} - S(x)}\right] - (n_z^{\,2} - S(x)) + \frac{D(x)^2}{n_y^{\,2} + n_z^{\,2} - S(x)}$$

The first term in C is antisymmetric in n_y and is proportional to the *gradients* of S and D; it is the term that causes the difference in coupling to the plasma for waves with n_y of opposite sign. For NSTX plasma parameters, the dD/dx term is the dominant one. When the pitch angle of the magnetic field relative to the horizontal is taken into account, a component of the up-down asymmetry in the local coordinate system becomes the right-left toroidal asymmetry observed in the experiments.

Figure 11 shows the magnitude of S_{pos} and S_{neg} computed by RANT3D/GLOSI for the same plasma conditions except for the pitch angle of the magnetic field. It indicates that the asymmetry is primarily caused by the large pitch angle of the magnetic field in front of the antennas, and equals zero for 0° pitch angle. Loading and coupling asymmetries have been qualitatively observed on many other tokamaks, but because the pitch angle is usually ≤ 15° the effect is fairly small. It is the characteristic large-pitch-angle operation of spherical torus plasmas that makes it so clearly observable in the NSTX rf experiments.

RANT3D/GLOSI computes the rf electric and magnetic fields in the antenna and at the surface of the plasma, which also shows the asymmetry. **Fig. 12** shows the magnitude of the toroidal B-field component (normalized) near the plasma surface vs. toroidal position for the case when only one current strap is driven. Three cases are plotted, the first being a normal plasma case with non-zero poloidal field (solid curve); the pitch angle of the total magnetic field at the surface of the Faraday shield is about 35° for this case. The second is a plasma case with zero poloidal field, in which the density profile used is the same as that for the previous case, the static poloidal field was set equal to zero, and the toroidal field was increased slightly so that $|B(x)|$ was the same for both cases. The third curve is for a vacuum case. The locations of three current straps are indicated in the plot, with the driven one in the center and an undriven one on either side. We see that the presence of the plasma causes a reduction in the field in front of the undriven straps, even when $B_y = 0$. When $B_y \neq 0$, the reduction is asymmetric, with the field decreasing more on the negative side (i.e., on the side with the lower-numbered strap).

7. Practical example and conclusions

The asymmetrical S-matrix can have a major effect on plasma loading when the antenna phasing is changed. A series of current drive (CD) experiments was carried out on NSTX in the Spring of 2002.[12, 13] Plasma parameters were I_p = 500 kA, B_0 = 0.45 T, $n_0 \approx 1.2 \times 10^{19}$ m^{-3}. Three phasings of the antenna array were used:

Symmetric phasing	ϕ = [0	0	π	π	0	0]
Co-current drive phasing	ϕ = [0	$-\pi/2$	$-\pi$	$-3\pi/2$	-2π	$-5\pi/2$]
Counter-current drive phasing	ϕ = [0	$\pi/2$	π	$3\pi/2$	2π	$5\pi/2$]

where the arrays above show the relative phasing of the rf voltage driving the six resonant loops. RF power levels for the experiments ranged from about 1 to 3 MW into the plasma.

The launched k_z spectra, calculated using measured density profiles and the GLOSI/RANT3D codes, are shown in **Fig. 13**. As can be seen the co-CD phasing launches largely monochromatic waves with the peak at $k_z \approx 8$ m^{-1}, the counter-CD spectrum is peaked in the opposite direction, and the symmetric phasing launches a spectrum with peaks at both +8 m^{-1} and -8 m^{-1}.

The analysis technique described in **Sec. 3** was used in conjunction with the measured density and magnetics information to calculate the 12 x 12 antenna S-matrix, which was then run through the circuit analysis code to compute the 6 x 6 S-matrix. Using this, the ratio of reflected to forward power could be computed for the different phasings given above. This was then translated to a load resistance, which is that resistance that one would have to terminate a 50-Ω line by to achieve the same value of reflected power/forward power in that line. **Fig. 14** shows a comparison of the experimental and calculated load resistances averaged over the sources. As can be seen, the agreement between the experimental and code-computed values is quite good, and indicates about a factor of two change in loading as one goes from counter-CD to co-CD phasing, even though the shape of the launched wave spectra are very similar, just in opposite directions. This large change in loading is a direct consequence of the S-matrix asymmetry described in this paper.

In summary, the large pitch angle of the magnetic field in NSTX and other spherical torii can introduce a significant difference in both the plasma loading of the antenna and the launched wave spectrum. This has a large effect on the practical aspects of tuning and matching the rf system to a plasma, and must be considered during design and operation of such systems. This asymmetry arises from an asymmetry inherent in the plasma dispersion relation when gradients in the plasma are taken into account, and is primarily a cold-plasma effect.

A technique has been developed and tested to measure the complete S-matrix of a multi-port antenna system in the presence of plasma. It provides a powerful method of measuring the complete S-matrix in a fairly short time interval during a plasma shot. Good agreement between measured an calculated values of the S-matrix components was obtained.

Finally, we have developed a technique to compute the complete n x n Z- or S-matrix of an antenna system. This provides a very useful tool, because once this matrix is available, the properties of the rf system can be computed for a range of different rf conditions (e.g., different loop powers and phasings) without performing any more plasma calculations.

Acknowledgements

The authors wish to thank the members of the NSTX team at PPPL and at collaborating institutions for their help in the operation of the machine and in the measurements of NSTX plasma properties. Particular thanks to E. Fredd, N. Greenough, and C. Brunkhorst for the operation and improvement of the ion cyclotron system, and to D. Mueller, R. Raman, and D. Gates for operation of the machine during these experiments.

This research was sponsored by the Office of Fusion Energy, U. S. Department of Energy, under contract DE-AC05-00OR22725 with Oak Ridge National Laboratory managed by UT-Battelle and under contract DE-AC02-76CH03073 with Princeton Plasma Physics Laboratory.

References

[1] M. Ono, *Phys. Plasmas* **2**, 4075 (1995).

[2] P. M. Ryan et al., in *Proc. 2nd Europhysics Topical Conf. on RF Heating and Current Drive of Fusion Devices,* Brussels, Belgium, (European Phys. Soc., 1998) p. 97.

[3] J. R. Wilson et al., in *Proc. 13th Topical Conf. on Radio Frequency Power in Plasmas,* Annapolis, MD (AIP Conf. Proc. 485, 1999), p. 168.

[4] D. W. Swain et al., in *Proc. 14th Topical Conf. on Radio Frequency Power in Plasmas,* Oxnard, CA (AIP Conf. Proc. 595, 2001), p. 154.

[5] M. D. Carter et al., *Nucl. Fusion* **36,** 209 (1996).

[6] C. Y. Wang, et al., *Phys. Plasmas* **2**, 2760 (1995).

[7] *Reference Data for Radio Engineers, Fifth Edition,* H. P. Western, ed. (Howard. W. Sam, 1974) Chap. 24.

[8] R. J. Maqueda et al., *Rev. Sci. Instr.* **72**, 931 (2001); R. J. Maqueda et al., *Rev. Sci. Instr.*, to be published (2003).

[9] J. B. Wilgen et al., *Bull. Am. Phys. Soc.* **46,** No. 8, p. 259 (2001)

[10] S. A. Sabbagh et al., *Nucl. Fusion* **41**, 1601 (2001).

[11] T. H. Stix, *Theory of Plasma Waves* (McGraw-Hill, 1962) Chap. 1

[12] D. W. Swain et al., in *Proc. 29th Conf. on Plasma Physics and Controlled Fusion*, Montreux, Switzerland 2002 (to be published).

[13] P. M. Ryan et al., in *Proc. 19th IAEA Fusion Energy Conf.* Lyon, France 2002 (to be published).

FIGURES

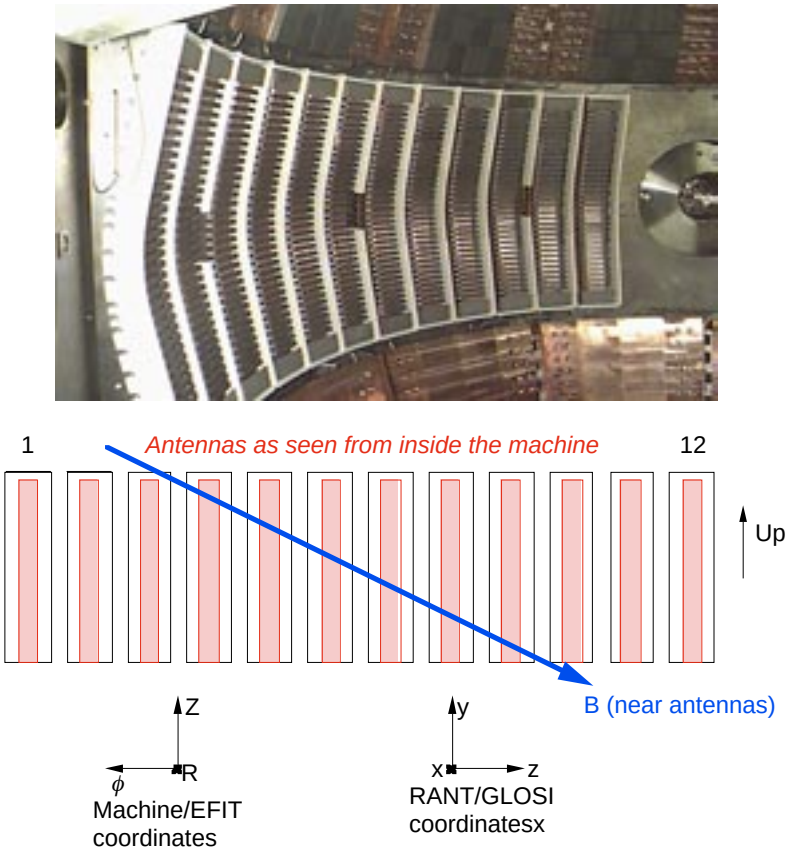

Fig. 1. Picture of the 12-strap antenna installed in NSTX (top), and a diagram showing typical B-field orientation (arrow, bottom).

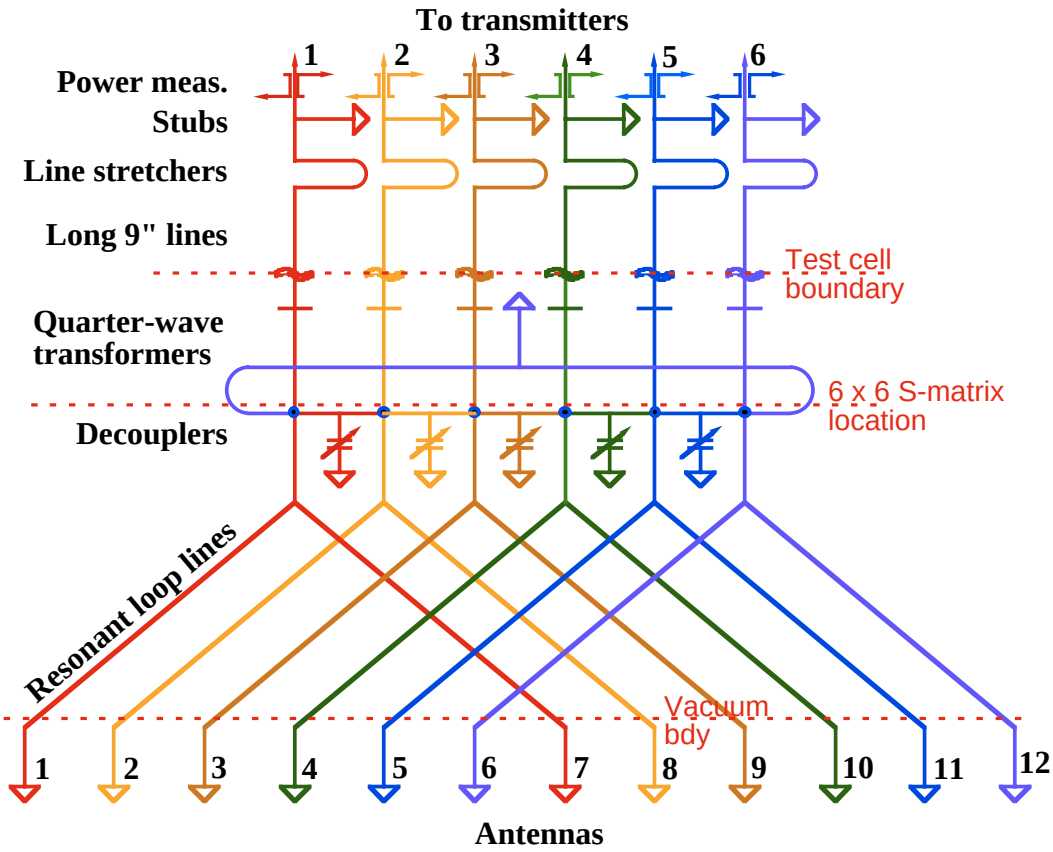

Fig. 2. Schematic of the NSTX rf system.

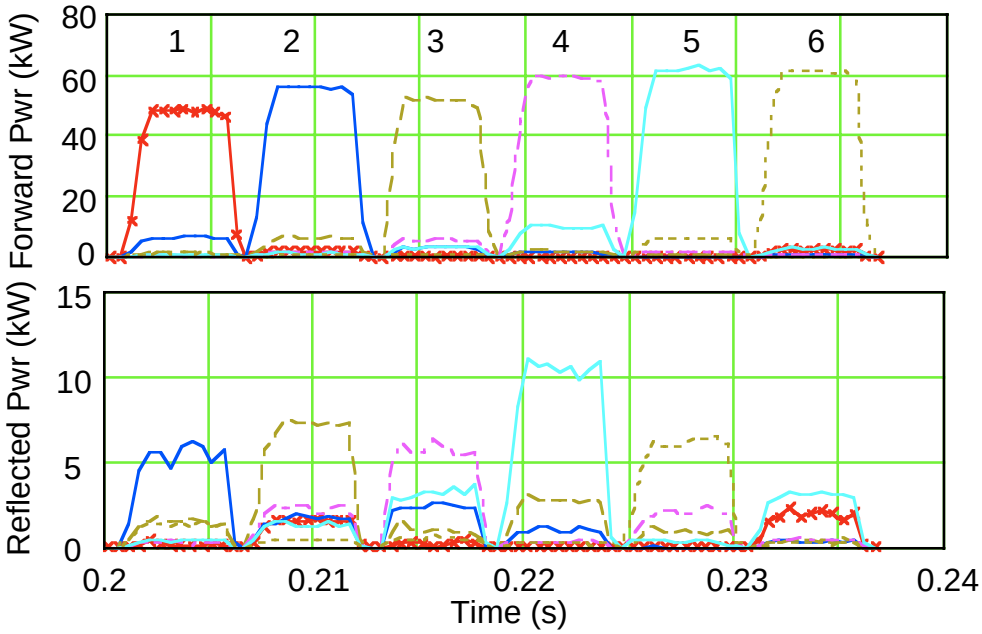

Fig. 3. Forward (top) and reflected (bottom) power vs. time as each of the six transmitters are sequentially pulsed.

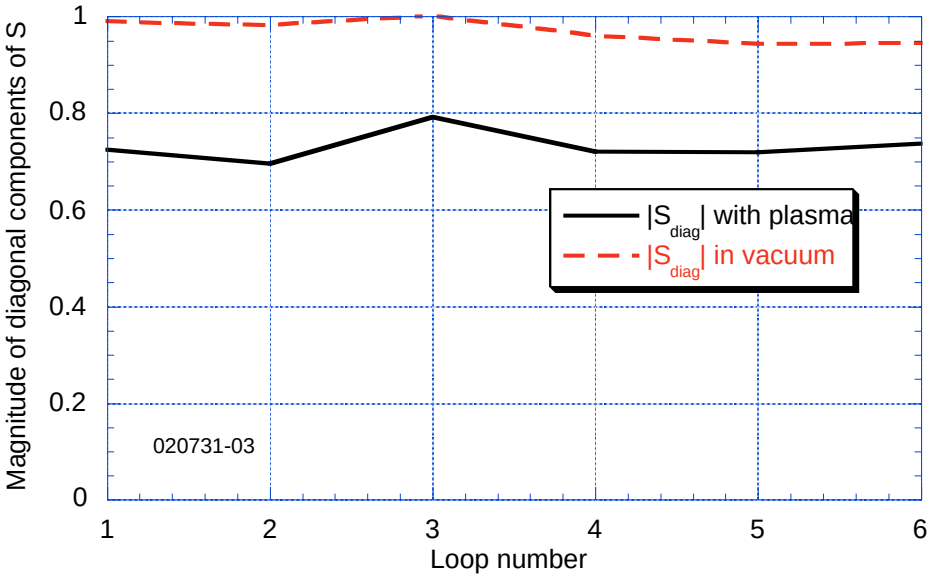

Fig. 4. Magnitude of diagonal components of S on the source side of the decouplers for plasma shot (105888) and vacuum shot (105760) vs. resonant loop number.

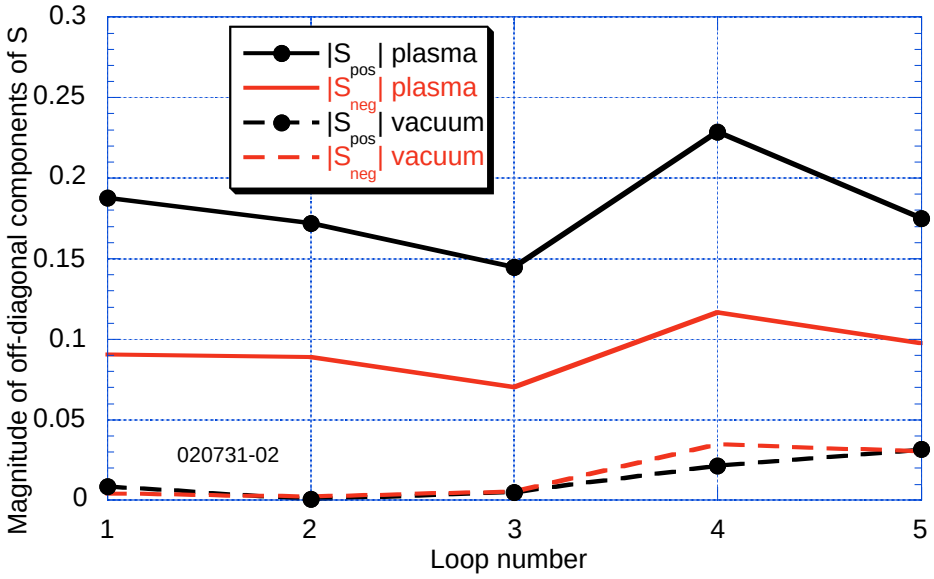

Fig. 5. Magnitude of off-diagonal components of S for plasma shot (solid curves) and vacuum shot (dashed curves).

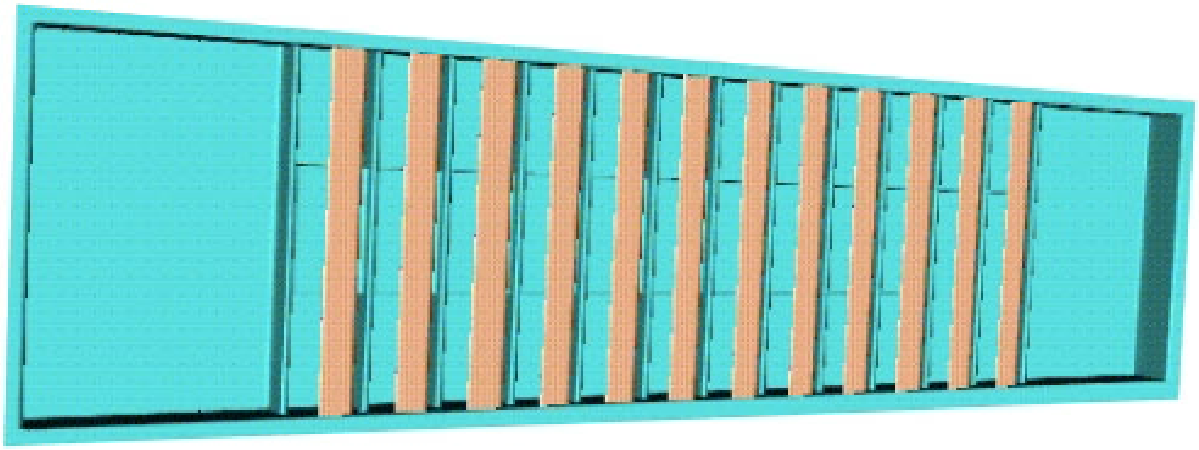

Fig. 6. Model of the NSTX 12-strap antenna used in RANT3D computations.

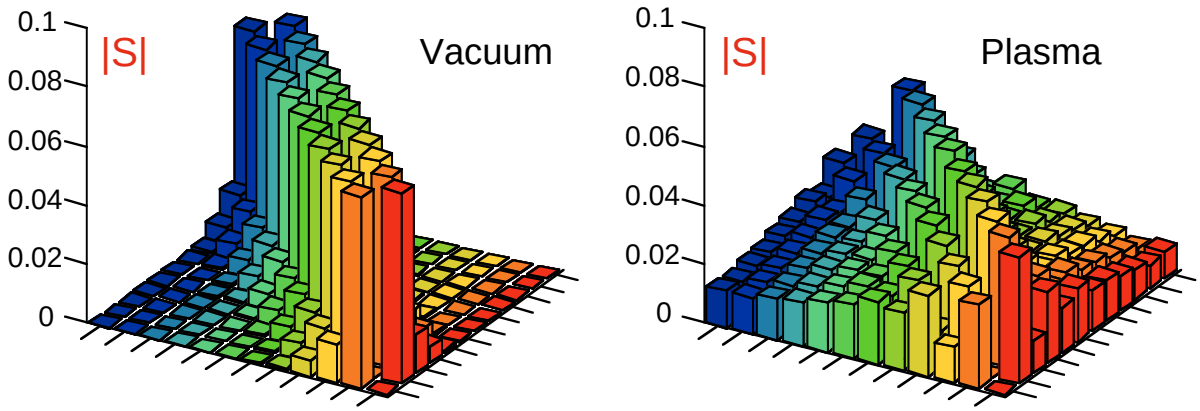

Fig. 7. Magnitude of the 12 x 12 S antenna S-matrix with no plasma (left) and for a typical plasma case (right). Diagonal terms in S are set equal to zero for these plots. Vacuum case shows symmetry across the diagonal, while the plasma case is not symmetric.

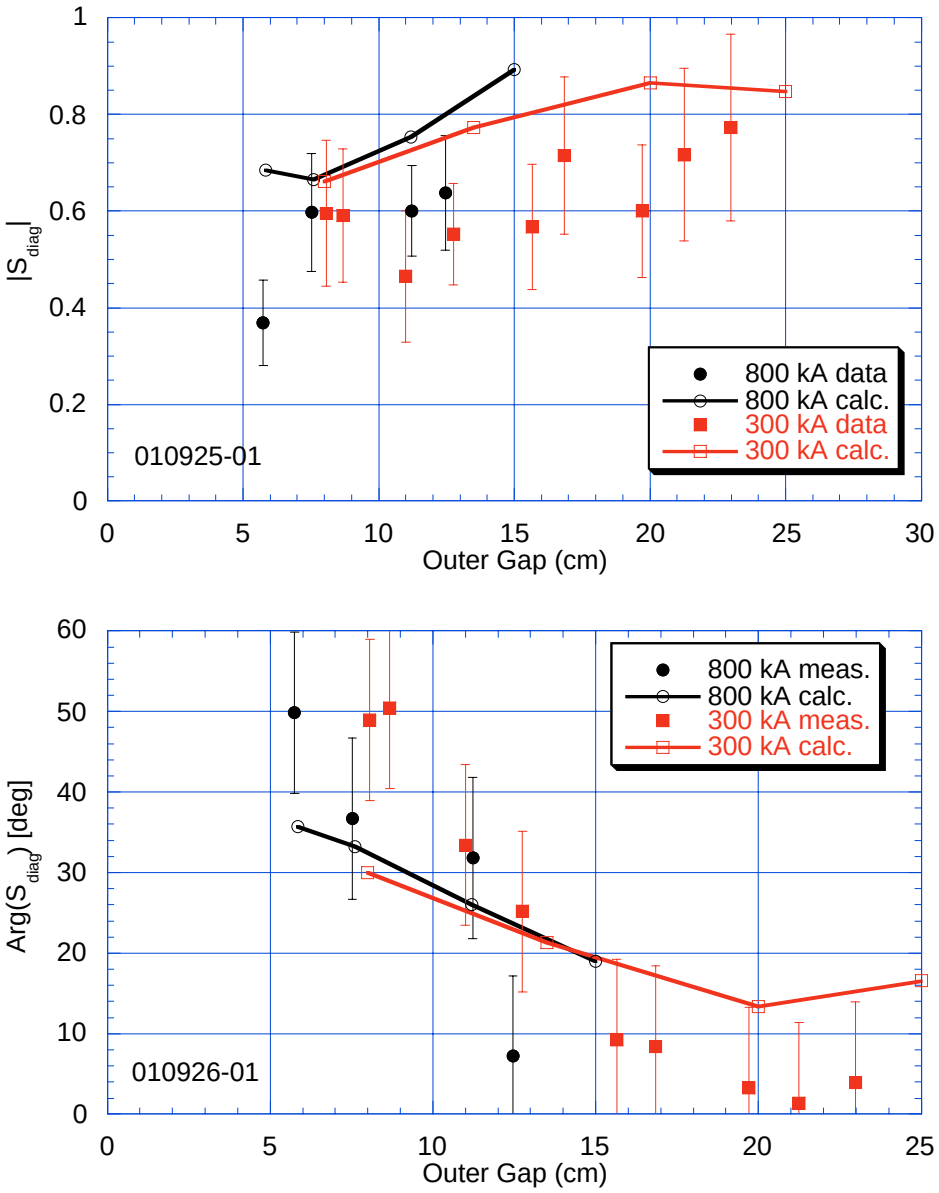

Fig. 8. Magnitude (top) and phase angle (bottom) of average diagonal component of S vs outer gap. Points are results of analysis of shots, while lines are RANT3D results.

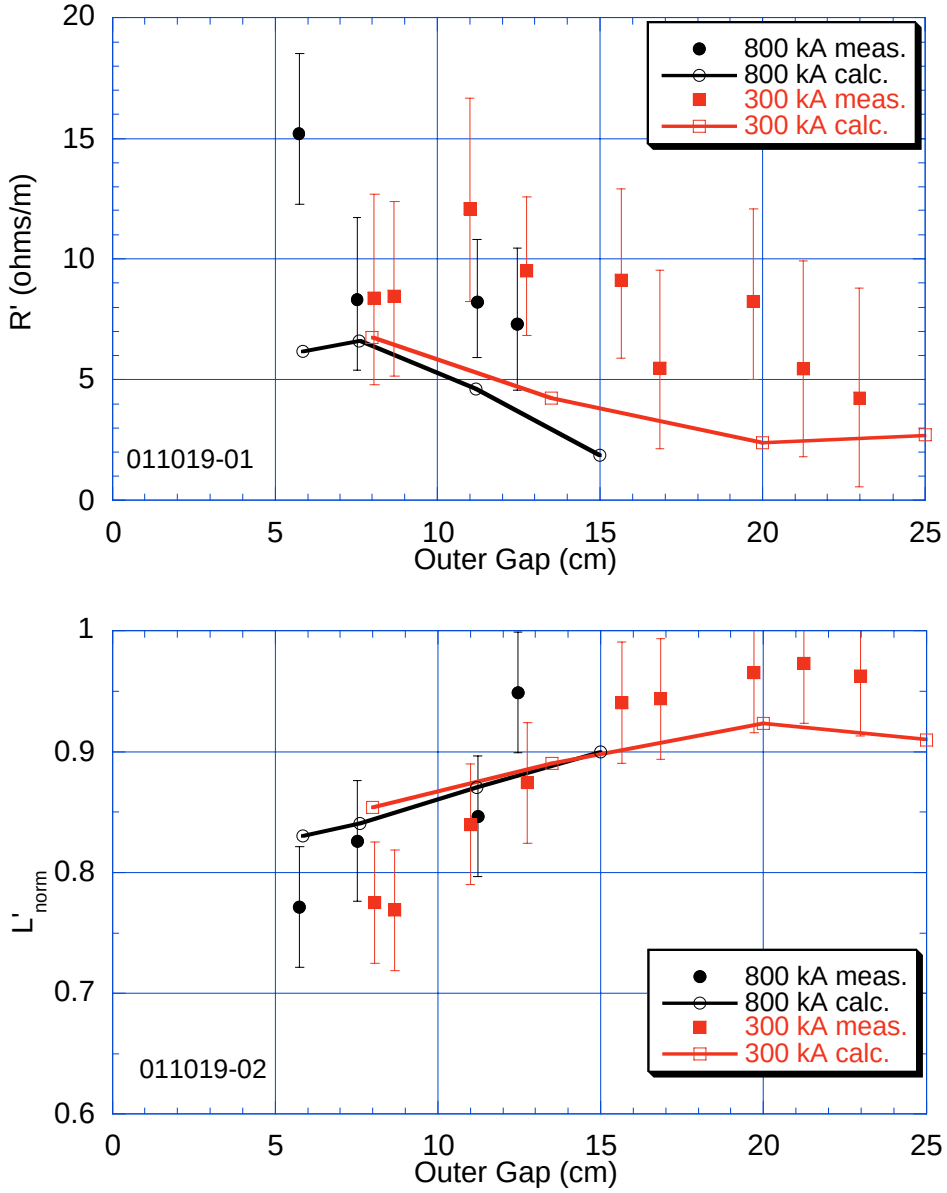

Fig. 9. Plasma load resistance (top) and relative strap inductance (bottom) vs. outer gap; $L'_{norm} = L'/L'_{vacuum}$.

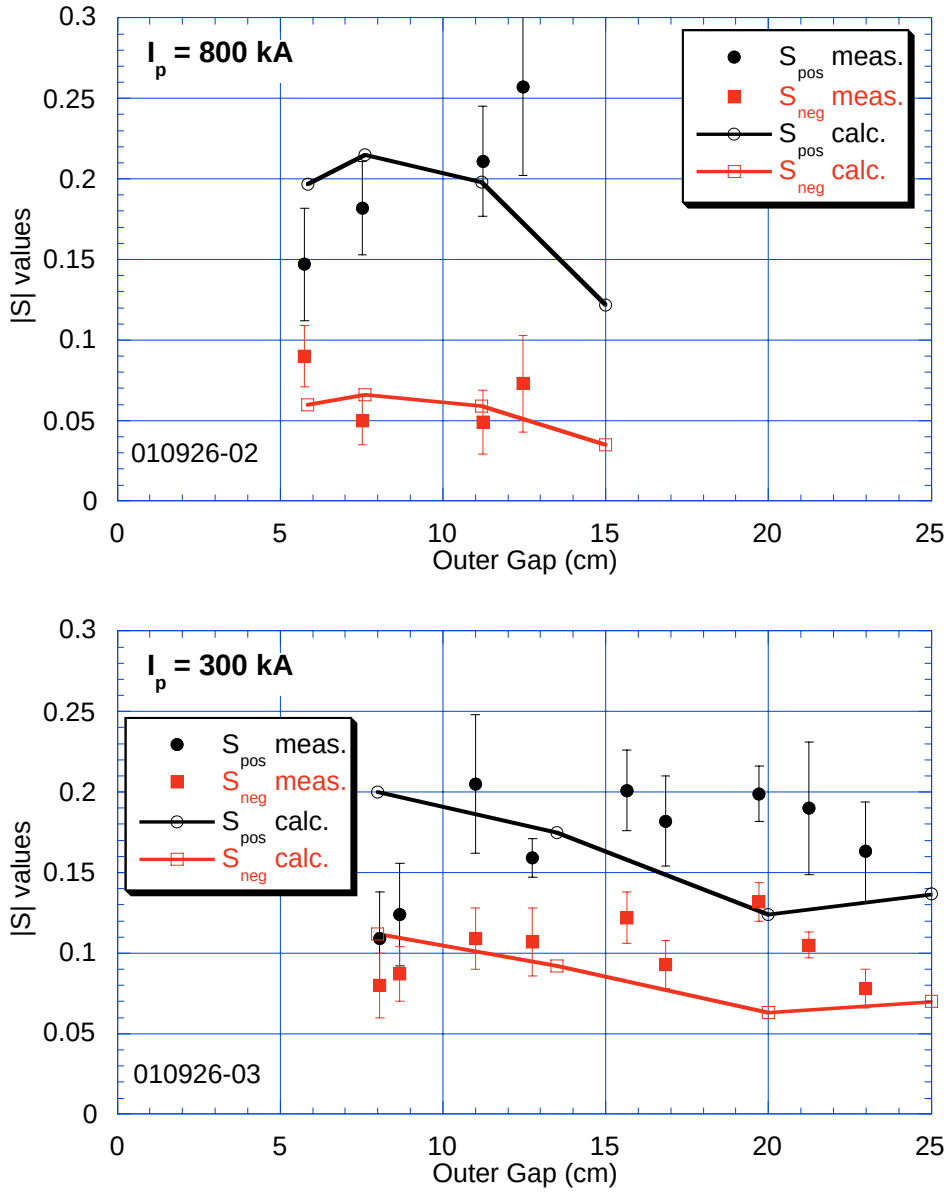

Fig. 10. Off-diagonal terms of S vs. gap, for both 800 kA(top) and 300 kA (bottom) shots.

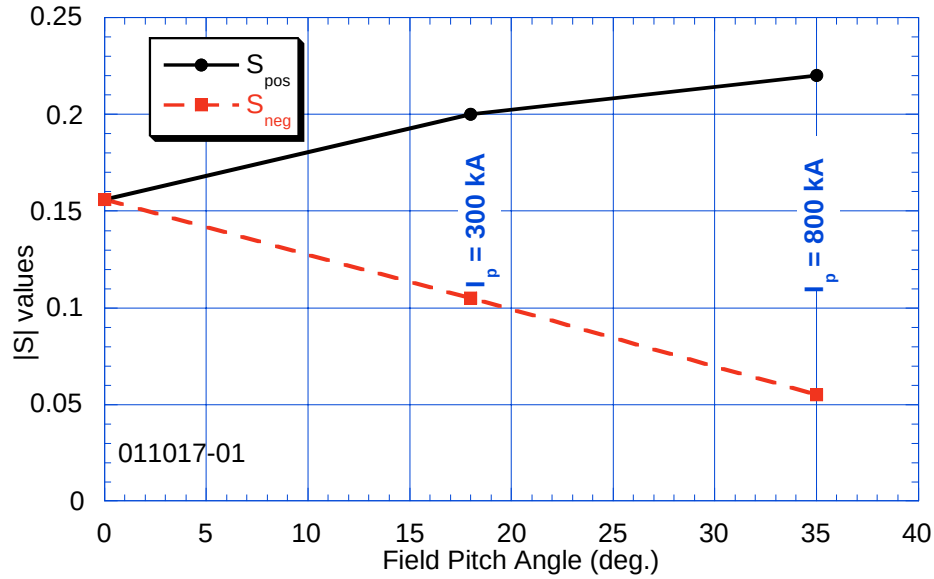

Fig. 11. Magnitude of the off-diagonal terms of the S-matrix as a function of magnetic field pitch angle.

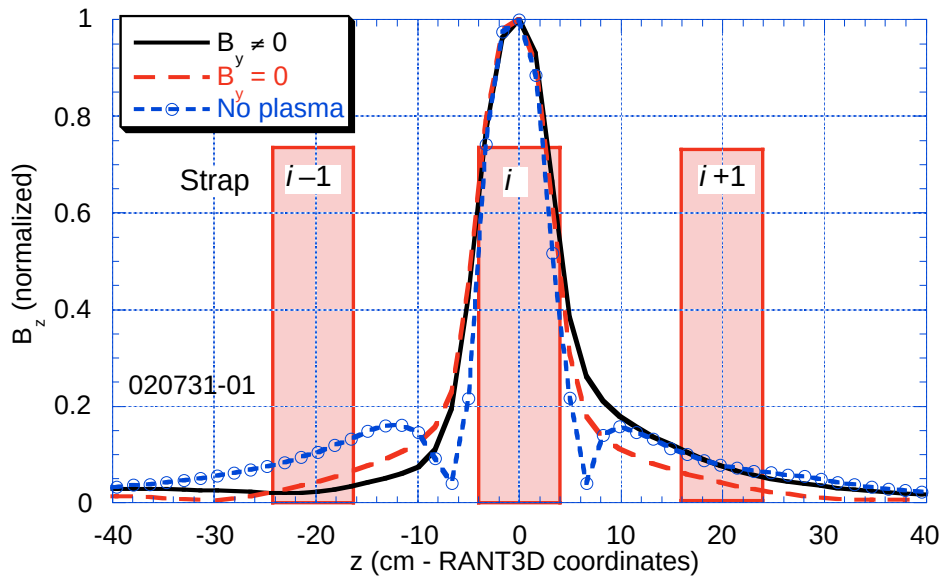

Fig. 12. Magnitude of toroidal (z) component of the rf field from one current strap computed for normal plasma conditions, plasma present with zero poloidal field, and no plasma.

angle.

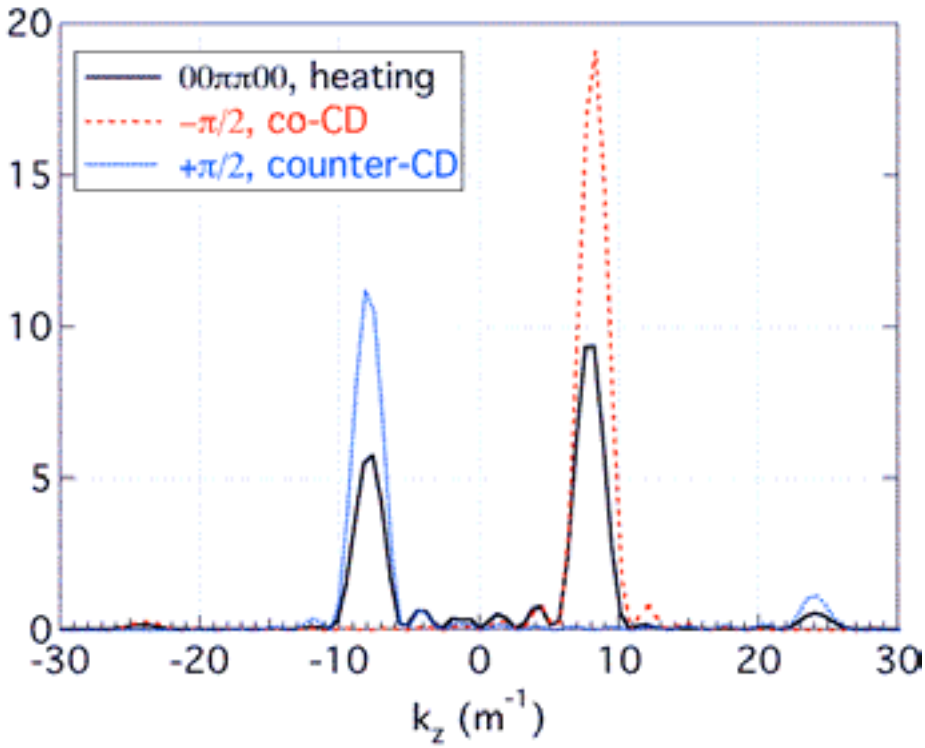

Fig. 13. Launched wave power vs. k_z for three antenna array phasings.

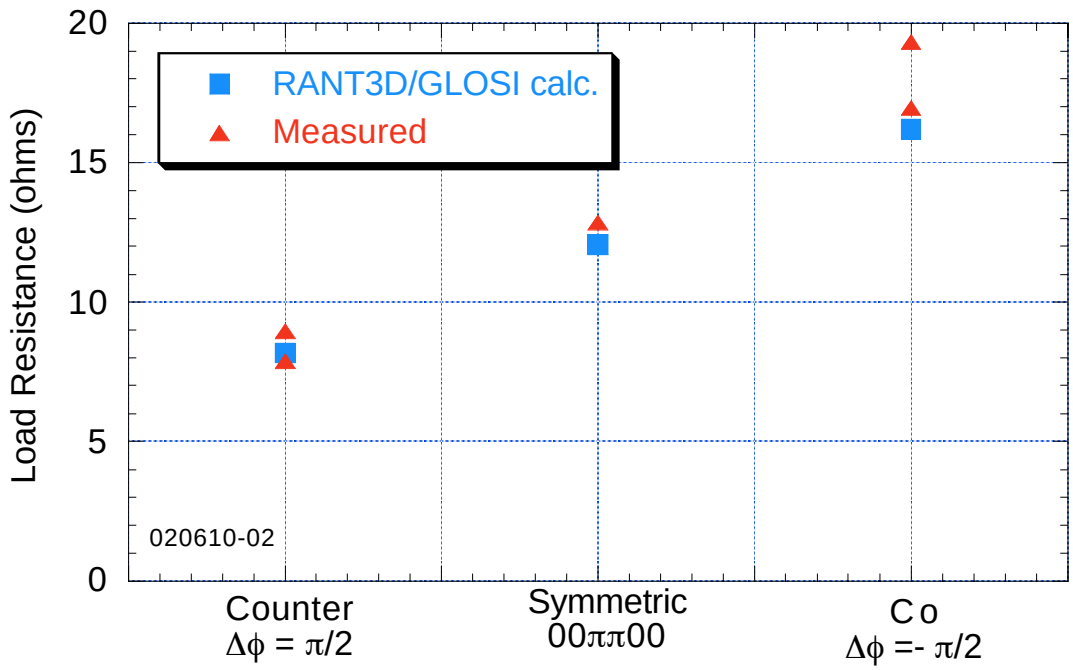

Fig. 14. Comparison of the average measured and calculated load resistance for three phasings.